Energy & Environmental Science

Accepted Manuscript

ROYAL SOCIETY OF CHEMISTRY

www.rsc.org/ees

Abnormal Crystal Growth in $CH_3NH_3PbI_{3-x}Cl_x$ Using a Multi-cycle Solution Coating Process

Qingfeng Dong, Yongbo Yuan, Yuchuan Shao, Yanjun Fang, Qi Wang and Jinsong Huang*[1]

Department of Mechanical and Materials Engineering and Nebraska Center for Materials and Nanoscience, University of Nebraska-Lincoln, Lincoln, Nebraska 68588-0656

Abstract: The efficiency of organolead trihalide perovskite solar cells has rocketed recently due to the improved material qualities with longer carrier diffusion lengths. Mixing chlorine in the precursor for mixed halide films was reported to dramatically enhance the diffusion lengths of mixed halide perovskite films, mainly due to the much longer carrier recombination lifetime. Here we report that adding Cl containing precursor for mixed halide perovskite formation can induce the abnormal grain growth behavior that yields well-oriented grains accompanied with appearance of some very large size grains. The abnormal grain growth becomes prominent only after multi-cycle coating of MAI:MACl blend precursor. The large grain size is found mainly to contribute to a longer carrier charge recombination lifetime, and thus increases the device efficiency to 18.9 %, but without significantly impacting the carrier transport property. The discovered strong correlation between material process and morphology provides guidelines for future material optimization and device efficiency enhancement.

*1 Correspondence should goes to Dr. Jinsong Huang at jhuang2@unl.edu.

Organolead trihalide perovskites (OTPs) are emerging as a new generation of solution processable photovoltaic materials which are low-cost and nature-abundant.[1-16] OTPs have shown intriguing optoelectronic properties for photovoltaic applications, such as strong absorption in ultraviolet-visible range, excellent crystallinity, bipolar carrier transport capability, and large charge diffusion length which enabled high performance perovskite photovoltaic devices (PPVs).[3,10,17,18] Methylammonium (MA) mixed lead halides, $CH_3NH_3PbX_{3-x}Y_x$ (X, Y = I, Br, Cl) attracted most attentions because of the high power conversion efficiency (PCE) of above 15% first achieved in PPVs with planar heterojunction (PHJ) structure.[1-16,19] It was later found that the diffusion length in mixed trihalide perovskite films in the order of 1 micrometer is ten times longer than that in triiodide perovskite films (~100 nm),[4] which is a significant discovery because a longer carrier diffusion length enables the application of thicker mixed trihalide perovskite films for stronger absorption. The ultra-long carrier diffusion length in mixed halide OTPs was mainly contributed by the much longer charge recombination lifetime.[4,20,21] However, the origin for the much longer diffusion length in mixed halide OTPs remains unclear from aspect of the material microscopic structure.

Here we report mixed halide perovskite films formed by a multi-cycle coating contain some very large mixed halide OTPs grains with preferred orientation due to a new grain growth mode (abnormal growth). A correlation between the film microstructure and electronic property and device performance was identified. High grain size: thickness ratio dramatically reduced grain boundary (GB) area and the associated charge recombination, which contributed to the improved device efficiency upto 18.9 %.

Cl was introduced from a mixed MAI:MACl precursor which has a much higher solubility than $PbCl_2$ in common solvents such as 2-propanol. Fig. 1a illustrates the multi-cycle solution deposition and thermal annealing induced interdiffusion processes of the PbI_2/ MAI:MACl films. A PbI_2 layer was first coated, and then MAI:MACl dissolved in an orthogonal solvent of 2-propanol was coated onto PbI_2, which was followed by a thermal annealing induced interdiffusion process to form homogeneous, pin-hole free perovskites films.[22] Here, the multi-cycle coating process was used for the first time for MAI:MACl precursor, which was found to be able to precisely control the amount of Cl incorporated in mixed halide OTPs. For each coating cycle, a drop of MAI:MACl precursor solution was dripped onto the center of the spinning substrate, and the precursor spread immediately. After the previous layer dried, another coating cycle was followed. The multi-cycle coating process enabled systematical control of the film thickness and mole ratio of the MAI:MACl and PbI_2 to form the stoichiometric mixed halide perovskite for an optimized device efficiency.

Figure 1b shows the wide spectral XRD patterns of annealed $MAPbI_{3-x}Cl_x$ films with different MAI:MACl coating-cycles. The crystal structure of the mixed halide perovskites still followed that of the $MAPbI_3$. One striking change of these diffraction patterns was the intensity of (220) peak at 28.7° increased significantly with more MAI:MACl coating-cycles, while the (310), (224), and (314) peaks at 32.0°, 41.0°, and 43.5° only changed a little. This indicates the crystal grains in the mixed halide perovskite films formed by this new method had oriented grains. In order to identify the origin of grain orientation change, a set of control samples were fabricated using MAI for the multi-cycle coating. Their XRD patterns of $MAPbI_3$ fabricated by multi-cycle coating were shown in Figure 1c. The ratio of peak intensity of (220) to (224) planes

was summarized in Figure 1d for these two types of films with and without Cl after different coating-cycles. There was a dramatic increase of the ratio of (220) / (224) peak intensity in $MAPbI_{3-x}Cl_x$ films, while barely no change in $MAPbI_3$ films, which is solid evidence that the grain orientation change is caused by the Cl added in the precursor.

The grain growth process was studied by scanning electron microscope (SEM) for the films formed with 280 nm PbI_2 reacted with different coating-cycles of MAI:MACl, and was found the preferred grain orientation originated from the abnormal grain growth behavior. The SEM images of the pervoskite films with 1, 4, 8 and 14 coating-cycles of MAI and MAI:MACl were shown in Fig. 2a-d, and the statistics of grain size derived from their SEM images (Fig. S1) were shown in Fig. 2e-f. The grain size in the $MAPbI_{3-x}Cl_x$ films was significantly enlarged, and some very large grains appeared in the perovskite films with the increased MAI:MACl coating-cycles. The grain size distribution histogram showed a transition from unimodal distribution to bimodal distribution for the $MAPbI_{3-x}Cl_x$ films. The grain size distribution histogram had only one peak in the films with single cycle MAI:MACl coating. However, the peak became broader and unsymmetrical with increased MAI:MACl coating-cycles, meanwhile, a new peak corresponding to the very large grains appeared, as labeled in the Fig. 2e. The size variation of the grains in these two peaks as well as the largest grains was summarized in Fig. 2e with respect to the MAI:MACl coating-cycles. With the increased MAI:MACl coating-cycles from 1 to 14, the average grain size increased 5.7 times from 228 nm to 1,210 nm, and the largest grain size increased from 500 nm to 3.3 micrometers. The thicknesses variation of the films with respect to the MAI:MACl coating-cycles were also included in Fig. 2f, which showed a quick increase in the first 4 coating-cycles and a slow saturation to 580 nm afterwards with the depletion of PbI_2. The average grain sizes are thus significantly larger than the film thicknesses after several

coating-cycles, and the largest grain size is 6 times of the corresponding film thickness. The much larger grain size than film thickness together with the appearance of elongated grain are features of an abnormal grain growth process in the mixed halide perovskite films.[23-25]

In order to find out the driving force of abnormal grain growth behavior, we examined the two possible origins, multi-cycle coating and Cl added in the precursor, by studying the grain growth behavior in the $MAPbI_3$ control samples fabricated the same as that of $MAPbI_{3-x}Cl_x$ samples. As shown in the SEM images in Fig. 2g-j, the multi-cycle coating process only slightly increased the grain size of $MAPbI_3$ from 174 nm to 273 nm with increased coating-cycle from 1 to 8, which can be explained by the multi-cycle coating process provided a longer duration of solvent environment to promote the longer range diffusion of precursor ions, as demonstrated by the solvent annealing method we used. In contrast, there was no very large grain in $MAPbI_3$ films, indicating Cl added in the precursor was the mainspring originating the abnormal grain growth behavior.

We come to a scenario that enlarged grain by Cl incorporation was correlated with the different crystallographic orientations in $MAPbI_{3-x}Cl_x$ compared with $MAPbI_3$. In a thin film growth process, the growth rate of a grain is determined by the Gibbs free energy of the precursor and formed perovskite, which includes not only chemical energy difference, but also the surface energy and interface energy (and therefore crystallographic orientation) of the grains.[23-25] Grains with some special crystallographic orientations can have smaller surface energy and are easier to grow.[23-25] Since $MAPbI_3$ is tetragonal which has less symmetry than cubic structures, there can be large difference in the surface energy between different crystal planes/facets. We speculated that (220) plane has the smallest surface energy or interfacial

energy because more grains have this orientation to minimize the total free energy of the system. With the increase of coating-cycles, the (220) oriented grains grew faster by consuming neighboring non-oriented grains, either by regular grain growth of grain attachment process. It resulted in the grain distribution shifting to large grain size, which was evidenced by the observed bimodal distribution as well as the significantly increased ratio between the XRD intensity of (220) peaks and that of the (310), (224), and (314) peaks with increased coating-cycles.[23-27] The addition of Cl in the precursor promotes the secondary grain growth can be explained by the slowed crystal formation process. It has been reported that Cl in the precursor causes the formation of intermediate phases[28], which is also observed by us in this study,[29] which reduces the crystallization of $MAPbI_3$. A quick formation of $MAPbI_3$ is expected to form randomly oriented grains due to the randomness in nucleation process, while a slowed crystallization allows the nucleus to adjust the orientation to minimize the total Gibbs free energy. Our recent study using additional solvent vapor treatment during the film nucleation process confirmed this scenario. [30] The multi-cycle coating process should contributed to the grain growth process instead of grain nucleation process for the larger grains formation, because most of the grains already are formed in the first few cycles of coating.

It should be emphasized that it was the first time that a secondary grain growth process in mixed halide perovskite films was identified. The average and largest grain sizes are ~1.1 and ~3.3 μm, respectively, which are 2 and 6 folds that of the corresponding film thicknesses. The large grain size: film thickness ratio was important for their application in polycrystalline thin film photovoltaic devices, because a decreased grain boundary area contributes decreased charge recombination. Since the average grain size is significantly larger than the film thickness, most

of the charge carrier can efficiently transport across the perovskite films in a single crystal grain and be collected without the need to across any grain boundary.[22]

The influence of Cl incorporation and multi-cycle coating on the photovoltaic device performance was investigated. All the photovoltaic devices have a structure of indium tin oxide (ITO) / poly(3,4-ethylenedioxythiophene) poly(styrenesulphonate) (PEDOT:PSS) /$MAPbI_3$ or $MAPbI_{3-x}Cl_x$ /[6,6]-phenyl-C61-butyric acid methyl ester (PCBM 10 nm)/C_{60} (20 nm)/2,9-dimethyl-4,7-diphenyl-1,10-phenanthroline (BCP, 7.5 nm) /Aluminum (Al, 100 nm) which is shown in Fig. 3a.[11,31] The device fabrication and measurement details can be found in experiment section. As shown by the cross-section SEM in Fig. 3b, all of them showed continuous, compact, pin-hole free perovskite films formed on PEDOT:PSS, allowing us to fabricate high performance devices at high yield. Since the photovoltaic devices performance can be changed by multiple factors including the Cl ratio in MAI:MACl precursor, organic and inorganic precursor ratio, and the perovskite film thickness, we did a systematic optimization by varying these parameters one by one to optimize the device performance. Here, the influence of Cl incorporation on the device performance was investigated by comparing $MAPbI_{3-x}Cl_x$ PPVs and $MAPbI_3$ based control devices with all conditions kept the same except to the organic precursors with PEDOT:PSS as hole transport layer (HTL). We first optimized devices by varying the MAI or MAI:MACl concentration for an appropriate amount of MAI or MAI:MACl increase between two cycles for the best device performance. As shown in Fig. 3c and d, both $MAPbI_3$ and $MAPbI_{3-x}Cl_x$ device showed best device performance with 2.4 wt% organic prcusour solution. At this concentration, MAI:MACl ratio varying from 8:1 to 2:1 was used in precursor and the best $MAPbI_{3-x}Cl_x$ devices achieved with MAI:MACl ratio of 4:1. The best

device performance was got after optimizing the active layer thickness by changing the starting PbI_2 layer thickness. The best coating-cycles were optimized for each parameter as shown in Fig. S2-4. The photocurrent (*J*)-*V* curves of the optimized PPVs based on $MAPbI_3$ as well as $MAPbI_{3-x}Cl_x$ was shown in Fig. 3 c-f. The optimized PCEs were reached with 7 coating-cycles for the $MAPbI_3$ PPVs and 8-10 cycles for the $MAPbI_{3-x}Cl_x$ PPVs with 2.4 wt% MAI:MACl (4:1 mol:mol) precursor. The optimized $MAPbI_3$ PPVs had a J_{SC} of 19.61 mA cm^{-2}, a *V*oc of 0.91 V, a Fill factor (*FF*) of 75.14 % and a PCE of 13.41 %, and the optimized $MAPbI_{3-x}Cl_x$ PPVs have a J_{SC} of 20.71 mA cm^{-2}, a V_{OC} of 0.97 V, a FF of 79.69 % and a PCE of 16.01 %. There were 5-10 % increase in V_{OC}, FF and J_{SC} in the $MAPbI_{3-x}Cl_x$ PPVs compared with $MAPbI_3$ PPVs, resulting ~20 % higher PCE as a result of Cl addition in the precursor.

To understand the origin of the enhanced performance for device based on $MAPbI_{3-x}Cl_x$ than $MAPbI_3$, the charge carrier lifetime and motility were measured, and corresponding charge diffusion lengths were calculated. Previously the free charge lifetime was mainly determined by spontaneous radiative charge recombination lifetime, which only gives the lower limit of charge recombination lifetime.[4] Here the charge carrier recombination lifetime in real device working condition is determined by impedance spectroscopy measurement as the product of the chemical capacitance and recombination resistance.[32] Fig. 4g show the Nyquist plot of the measured and fitted impedance spectra of the $MAPbI_3$ and $MAPbI_{3-x}Cl_x$ devices with PEDOT:PSS HTL respectively. The equivalent circuit used to fit the measured impedance spectra is shown in Fig. S6. The charge carrier lifetime at short circuit condition is 18.3 μs for $MAPbI_{3-x}Cl_x$ devices which is longer than 10.5 μs for the $MAPbI_3$ devices, however the difference of carrier

recombination lifetime induced by Cl incorporation is much less than what reported previously. The longer recombination lifetime indicates the decrease of charge recombination which confirms our scenario that the large ratio of grain size to the thickness for the thin film is beneficial in reducing charge recombination. The reduced charge recombination explained the higher V_{OC}, FF and J_{SC} in the $MAPbI_{3-x}Cl_x$ devices. The charge extraction time (τ) of $MAPbI_{3-x}Cl_x$ and $MAPbI_3$ devices was derived by fitting the transient photocurrent decay curve with single exponential decay function, and was normalized by the film thickness and built-in potential, as shown in Fig. 4h. It is noted the measured τ is determined by the mobilities of both perovskite layer and the charge transport layers such as fullerene and BCP. Nevertheless, the τ variation should reflect the transport property change of the perovskite layers because the electron transport layers were the same. The τ of $MAPbI_3$ films decreased initially with coating-cycles, and then increased after 8 coating-cycles. In contrast, the τ kept increasing in $MAPbI_{3-x}Cl_x$ films with increased coating-cycles, indicating increasing carrier mobility. The lower carrier mobility in both types of perovskite films with less than 8 coating-cycles could be caused by residual PbI_2 which retards the charge collection from the perovskite layers. The $MAPbI_{3-x}Cl_x$ and $MAPbI_3$ films, which led to the optimized device efficiency, have comparable carrier mobility. This indicates that transport property was not improved by Cl incorporation despite the better alignment of the grain orientation. It suggests that the function of Cl incorporation mainly caused microstructure change of perovskite film with larger grain formed, which reduces charge recombination.

Photocurrent hysteresis was found in many perovskite PPVs, which possessed a serious hindrance for the development of PPVs and accurate characterization of the device efficiencies.

To find out whether there is photocurrent hysteresis[33] in our devices, we measured the transient response of the devices, and scanned the photocurrents with increasing or decreasing voltage. As shown in Fig. S5a, the photocurrents rose quickly to maximum in sub-millisecond which limited by the spin-rate of our chopper. It was verified by the same response curve by replacing the PPV devices with the silicon diode (Hamamatsu S1133). The fast photoresponse of PPVs indicates there was a low trap density in the optimized perovskite films or at the interfaces of the devices. As shown in Fig. S5b, no obvious photocurrent hysteresis was observed in our optimized devices by changing the photocurrent sweep rates from 0.15 V/s to 0.3 V/s or the sweep directions. The stabilized efficiency is the same as measured from *J-V* curve (Fig. 3i, J). Another merit of the multi-cycle coating method to fabricate mixed halide PPVs is that it gives an easy way to reproduce the optimized devices because of the precise control of the optimized ratio of MAI:MACl to PbI_2, which provide an excellent yield of high PCE devices. The statistics of the *FF*, V_{OC}, J_{SC} and PCE based on 30 mixed halide PPVs with PEDOT:PSS as HTL from five batches were shown in Fig. S5c-f which showed a high average *FF* of 79% and a highest PCE of 16.01% for the device fabricated on PEDOT:PSS.

Finally poly[bis(4-phenyl)(2,4,6-trimethylphenyl)amine] (PTAA) was recently shown by us to be a better HTL than PEDOT:PSS due to its larger work function and non-wetting surface.[34,35] We replaced PEDOT:PSS by PTAA, and conducted the same device optimization. The *J-V* curves as well as their external quantum efficiency (EQE) spectra of optimized devices based on PTAA was shown in Fig. 4. The device with PTAA has a much large V_{OC} to 1.1 V and slightly improved J_{SC} to 21.96 mA/cm^2, resulting a highest device efficiency of 18.9 %. Similarly these devices show very small photocurrent hysteresis when reverse the current scanning direction and

rate. The large J_{SC} is consistent with the integrated photocurrent of 21.24 mA cm^{-2} from the EQE (Fig. 4b).

In conclusion, we presented a comprehensive study on the mechanism of enhanced carrier diffusion length in mixed halide perovskite by revealing the correlation of fabrication process, material grain growth, composition, microstructure, and electronic properties. Using the multi-cycle interdiffusion method, a strong correlation was observed between the abnormal grain growth, grain lateral size/thickness ratio enhancement and carrier lifetime/diffusion length increase. The multi-cycle interdiffusion method to fabricate mixed halide perovskite films is a completely different method from the single step method reported previously in its different capability in controlling morphology and microstructures. The study presented here pointed out a new direction to produce very large size grains by abnormal grain growth mechanism, which is crucial to achieve high efficiency polycrystalline thin film solar cells because reduced grain boundary area can effectively reduce charge recombination. The film fabrication should not be limited to solution process because continuous evaporation of Cl containing precursor is also feasible by vapor deposition.

Methods:

PbI_2 and MAI:MACl precursor preparation:

MAI was synthesized using the method described by Michael M. Lee, et. al.[5] MACl was synthesized by the reaction of Methylamine (13.5 ml, 40% w/w aq. soln., Alfa Aesar) with a concentrated aqueous solution of Hydrochloric acid (23.5 mL, 36.5 wt% in water, Alfa Aesar) at 0 °C for 2 h with constant stirring under nitrogen atmosphere followed by a crystalized,

purification and dry process which was the same as the preparation of MAI. MAI:MACl precursor was prepared by mixing MAI and MACl in 2-propanol for different blend ratio and concentration. PbI_2 precursor was prepared by dissolving PbI_2 in DMF.

Film and photovoltaic device fabrication:

For perovskite films fabrication, all solutions were string at 100^{o}C to achieve fully dissolve before use. First, the PbI_2 hot solution was spun onto a PEDOT:PSS or PTAA coated ITO glass substrate. Then MAI or MAI:MACl solution was dipped on to the previous layers during the spinning of substrate after the previous layer dry for multi-cycle coating. The substrate was keep continues spinning during the whole multi-cycles and the previous layer will dry after continues spinning for 3 seconds after the solution spread for each cycle. In this work, 10 µl of 2.4 wt% MAI or MAI:MACl (4:1 mol:mol) solution was dipped onto the PbI_2 film at 6000 rpm and followed by dipping another 10 µl of MAI or MAI:MACl (4:1 mol:mol) onto previous layers every 3 second during continues spinning of substrate. After the coating of MAI or MAI:MACl, the film was transferred onto 60 $^{\circ}$C hotplate. For perovskite films with PEDOT:PSS HTL, 20 µl DMF was added into the petri dish covered on samples before annealing process and then for a 90 min solvent assistant thermal annealing at 110 ^{o}C. For perovskite films with PTAA HTL, lower annealing temprerature of 60 ^{o}C were used. For photovoltaic devices, 2 wt % solution of PCBM in DCB was spun onto the annealed perovskite film and followed by additional 60 min annealing. Then the device was completed by sequence depositing 20 nm C60, 7.5 nm BCP and 100 nm Al. The device J-V curve measurement was conducted in nitrogen filled glove-box.

Film and device characterization:

XRD measurements were performed with a Rigaku D/Max-B X-ray diffractometer with Bragg-Brentano parafocusing geometry, a diffracted beam monochromator, and a conventional copper target x-ray tube set to 40 KV and 30 mA. The single path absorption was measured using an Evolution 201 UV-Visible spectrometer (thermo Scientific). A Quanta 200 FEG Environmental Scanning Electron Microscope (ESEM) using a field-emission gun (FEG) electron source was used to scan the film morphology. The films were first covered with a thin layer of gold coated using a Cressington 108 Auto Sputter Coater before the SEM measurement. The photocurrent curves were measured under simulated AM 1.5G irradiation (100 mW/cm^2) using a Xenon-lamp- based solar simulator (Oriel 67005, 150 W Solar Simulator). A Schott visible-colour glass- filtered (KG5 colour-filtered) Si diode (Hamamatsu S1133) was used to calibrate the light intensity before photocurrent measurement to avoid optical mismatch. Impedance spectroscopy was recorded under AM 1.5G illumination by the E4980A Precision LCR Meter at frequency from 0.2 to 2000 kHz from Agilent with homemade software. The device area was 9 mm^2.

Acknowledgements

We thank the financial support from Department of Energy under Award DE-EE0006709 and National Science Foundation under Awards ECCS-1252623.

Reference

(1) Kojima, A.; Teshima, K.; Shirai, Y.; Miyasaka, T. *Journal of the American Chemical Society* **2009**, 131, 6050.

(2) Ball, J. M.; Lee, M. M.; Hey, A.; Snaith, H. J. *Energ Environ Sci* **2013**, 6, 1739.

(3) Xing, G.; Mathews, N.; Sun, S.; Lim, S. S.; Lam, Y. M.; Grätzel, M.; Mhaisalkar, S.; Sum, T. C. *Science* **2013**, 342, 344.

(4) Stranks, S. D.; Eperon, G. E.; Grancini, G.; Menelaou, C.; Alcocer, M. J.; Leijtens, T.; Herz, L. M.; Petrozza, A.; Snaith, H. J. *Science* **2013**, 342, 341.

(5) Lee, M. M.; Teuscher, J.; Miyasaka, T.; Murakami, T. N.; Snaith, H. J. *Science* **2012**, 338, 643.

(6) Rath, A. K.; Bernechea, M.; Martinez, L.; de Arquer, F. P. G.; Osmond, J.; Konstantatos, G. *Nat Photonics* **2012**, 6, 529.

(7) Marchioro, A.; Teuscher, J.; Friedrich, D.; Kunst, M.; Van De Krol, R.; Moehl, T.; Grätzel, M.; Moser, J.-E. *Nat Photonics* **2014**, 8, 250.

(8) Malinkiewicz, O.; Yella, A.; Lee, Y. H.; Espallargas, G. M.; Graetzel, M.; Nazeeruddin, M. K.; Bolink, H. J. *Nat Photonics* **2014**, 8, 128.

(9) Liu, D.; Kelly, T. L. *Nat Photonics* **2013**, 8, 133.

(10) Heo, J. H.; Im, S. H.; Noh, J. H.; Mandal, T. N.; Lim, C.-S.; Chang, J. A.; Lee, Y. H.; Kim, H.-j.; Sarkar, A.; Nazeeruddin, M. K. *Nat Photonics* **2013**, 7, 486.

(11) Leijtens, T.; Eperon, G. E.; Pathak, S.; Abate, A.; Lee, M. M.; Snaith, H. J. *Nat Commun* **2013**, 4, 2885.

(12) Kim, H.-S.; Mora-Sero, I.; Gonzalez-Pedro, V.; Fabregat-Santiago, F.; Juarez- Perez, E. J.; Park, N.-G.; Bisquert, J. *Nat Commun* **2013**, 4, 2242.

(13) Liu, M.; Johnston, M. B.; Snaith, H. J. *Nature* **2013**, 501, 395.

(14) Chung, I.; Lee, B.; He, J.; Chang, R. P.; Kanatzidis, M. G. *Nature* **2012**, 485, 486.

(15) Burschka, J.; Pellet, N.; Moon, S.-J.; Humphry-Baker, R.; Gao, P.; Nazeeruddin, M. K.; Grätzel, M. *Nature* **2013**, 499, 316.

(16) Chen, Q.; Zhou, H.; Hong, Z.; Luo, S.; Duan, H.-S.; Wang, H.-H.; Liu, Y.; Li, G.; Yang, Y. *Journal of the American Chemical Society* **2013**, 136, 622.

(17) Hodes, G. *Science* 2013, 342, 317.

(18) Docampo, P.; Ball, J. M.; Darwich, M.; Eperon, G. E.; Snaith, H. J. *Nat Commun* **2013**, 4, 2761.

(19) Lotsch, B. V. *Angewandte Chemie International Edition* **2014**, 53, 635.

(20) Edri, E.; Kirmayer, S.; Henning, A.; Mukhopadhyay, S.; Gartsman, K.; Rosenwaks, Y.; Hodes, G.; Cahen, D. *Nano Lett* **2014**, 14, 1000.

(21) Colella, S.; Mosconi, E.; Fedeli, P.; Listorti, A.; Gazza, F.; Orlandi, F.; Ferro, P.; Besagni, T.; Rizzo, A.; Calestani, G. *Chem Mater* **2013**, 25, 4613.

(22) Xiao, Z.; Bi, C.; Shao, Y.; Dong, Q.; Wang, Q.; Yuan, Y.; Wang, C.; Gao, Y.; Huang, J. *Energ Environ Sci* **2014**, 7, 2619.

(23) Thompson, C. V.; Carel, R. *Journal of the Mechanics and Physics of Solids* **1996**, 44, 657.

(24) Thompson, C. V. *Annual Review of Materials Science* **2000**, 30, 159.

(25) Thompson, C. V. *Annual Review of Materials Science* **1990**, 20, 245.

(26) Liang, P. W.; Chueh, C. C.; Xin, X. K.; Zuo, F.; Williams, S. T.; Liao, C. Y.; Jen, A. K. Y. *Advanced Energy Materials* **2015**, 5, 1400960.

(27) Qiu, J.; Qiu, Y.; Yan, K.; Zhong, M.; Mu, C.; Yan, H.; Yang, S. *Nanoscale* **2013**, 5, 3245.

(28) Zhang, W.; Saliba, M.; Moore, D. T.; Pathak, S. K.; Hörantner, M. T.; Stergiopoulos, T.; Stranks, S. D.; Eperon, G. E.; Alexander-Webber, J. A.; Abate, A. *Nat Commun* **2015**, 6, 6142.

(29) Jungseok Chae; Qingfeng Dong; Jinsong Huang; Andrea, C., unpublished.

(30) Lian, J.; Wang, Q.; Yuan, Y.; Shao, Y.; Huang, J. *J Mater Chem A* **2015** DOI: 10.1039/C5TA01595B.

(31) Wang, Q.; Shao, Y.; Dong, Q.; Xiao, Z.; Yuan, Y.; Huang, J. *Energ Environ Sci* **2014**, 7, 2359.

(32) Bisquert, J.; Fabregat-Santiago, F.; Mora-Seró, I. n.; Garcia-Belmonte, G.; Giménez, S. *The Journal of Physical Chemistry C* **2009**, 113, 17278.

(33) Snaith, H. J.; Abate, A.; Ball, J. M.; Eperon, G. E.; Leijtens, T.; Noel, N. K.; Stranks, S. D.; Wang, J. T.-W.; Wojciechowski, K.; Zhang, W. *The Journal of Physical Chemistry Letters* **2014**, 5, 1511.

(34) Deng, Y.; Peng, E.; Shao, Y.; Xiao, Z.; Dong, Q.; Huang, J. *Energ Environ Sci* **2015**, DOI: 10.1039/C4EE03907F.

(35) Bi, C.; Wang, Q.; Shao, Y.; Yuan, Y.; Xiao, Z.; Huang, J., *Nature Commun* in press.

Figure caption:

Figure 1. (a) Schematics of the formation of $MAPbCl_yI_{3-y}$ perovskite layer from multiple stacking layers of PbI_2 and MAI:MACl; (b-c)The XRD patterns of the $MAPbI_{3-x}Cl_x$ and $MAPbI_3$ films annealed at 110 ^oC for 90 min with different coating-cycles of MAI:MACl or MAI. (d) Intensity ratio of (220)/(224) peaks in the annealed $MAPbI_3$ and $MAPbI_{3-x}Cl_x$ films with different coating-cycles of MAI or MAI:MACl.

Figure 2. (a-d) SEM images of the pervoskite films with varied layers of MAI:MACl. (e) Statistics of grain sizes in 17 μm × 17 μm E images of the pervoskite films with varied coating-cycles of MAI:MACl. (f) Film thickness and grain size with respect to the different coating-cycles of MAI:MACl. (h-k) SEM images of the pervoskite films with varied coating-cycles of MAI

Figure 3. (a) Device structure of perovskite solar cells. (b) SEM image of the crosscection of a $MAPbI_{3-x}Cl_x$ perovskite film. (c-f) J-V curves for optimized multi-cycle coating interdiffusion processed perovskite solar cells based on (c) PbI_2 and MAI precursor with different concentration; (d) PbI_2 and MACl:MAI precursor with different concentration and (e) different MACl:MAI ratio; (f) MACl:MAI (2.4 wt%, mol:mol 1:4) and PbI_2 layer with different thickness. (g) Nyquist plot of impedance spectra of $MAPbI_3$ (red dot) and $MAPbI_{3-x}Cl_x$ (blue dot) devices, respectively. Dots are measured results and lines are fitted curves. (h) Charge extraction time of optimized $MAPbI_3$ and $MAPbI_{3-x}Cl_x$ perovskite photovoltaic devices with varied coating-cycles. (i) J-V curve of the optimized $MAPbI_{3-x}Cl_x$ perovskite photovoltaic devices on PEDOT:PSS and (j) Steady-state photocurrent output at the maximum power point (0.80 V).

Figure 4. (a) J-V curves for optimized multi-cycle coating interdiffusion processed $MAPbI_{3-x}Cl_x$ perovskite solar cells on PTAA and (b) the EQE spectra.

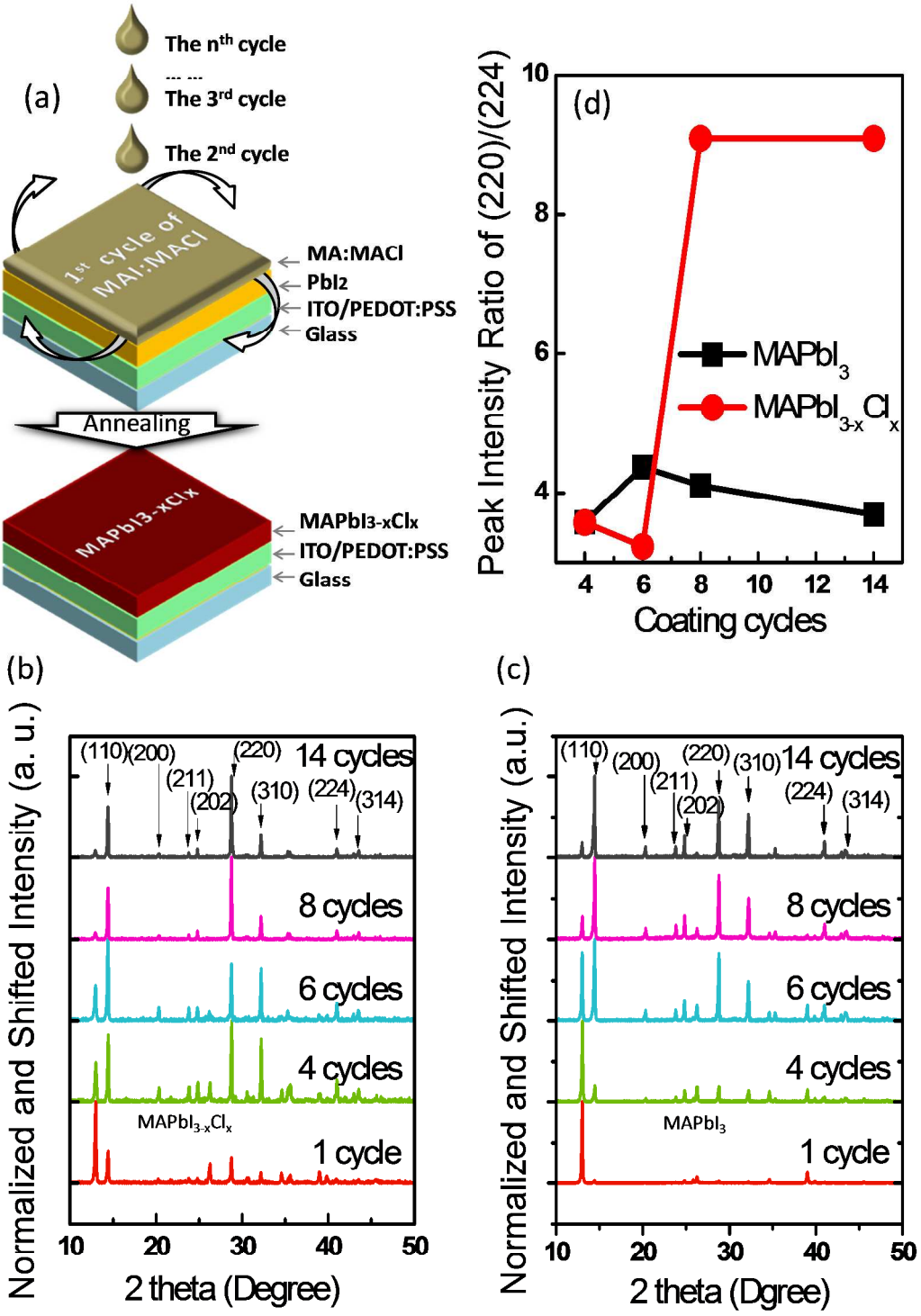

Figure 1. *Q. Dong et al*

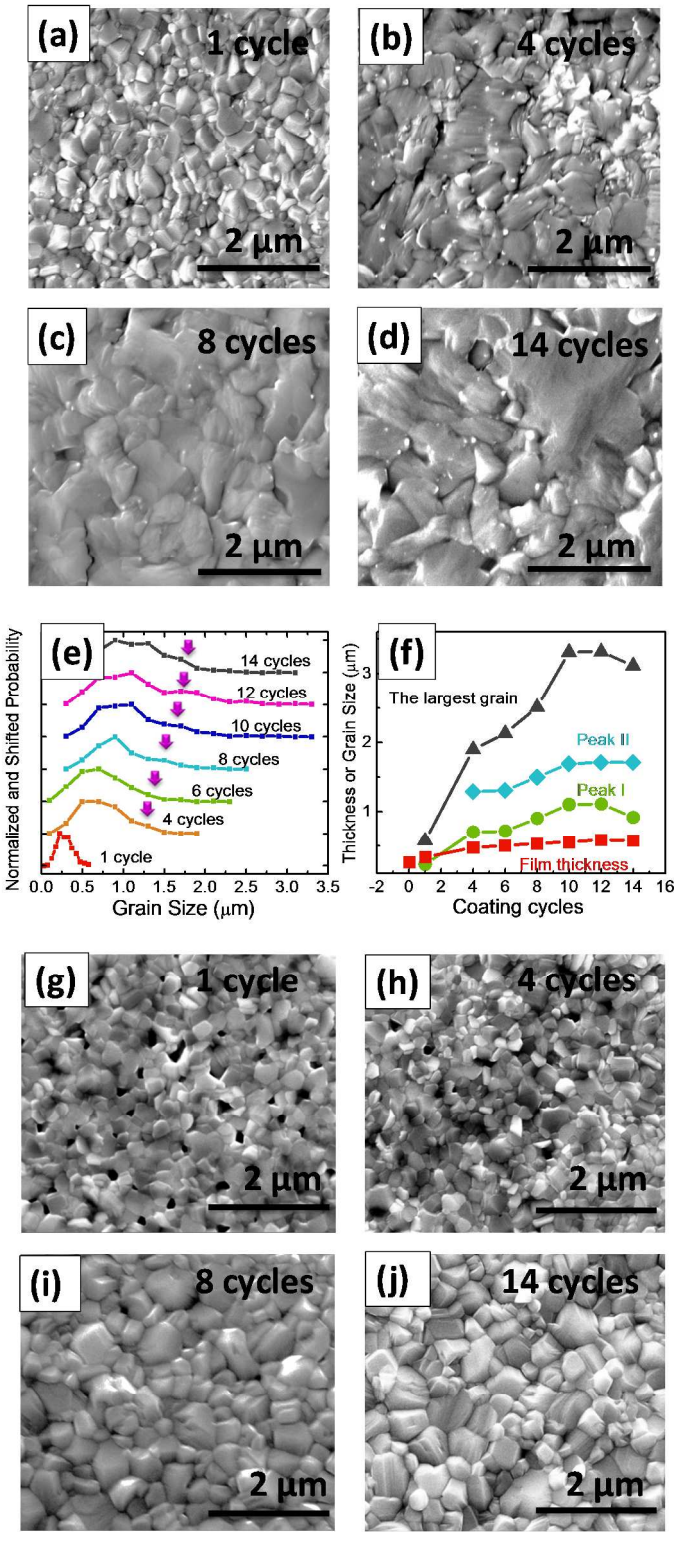

Figure 2. *Q. Dong et al*

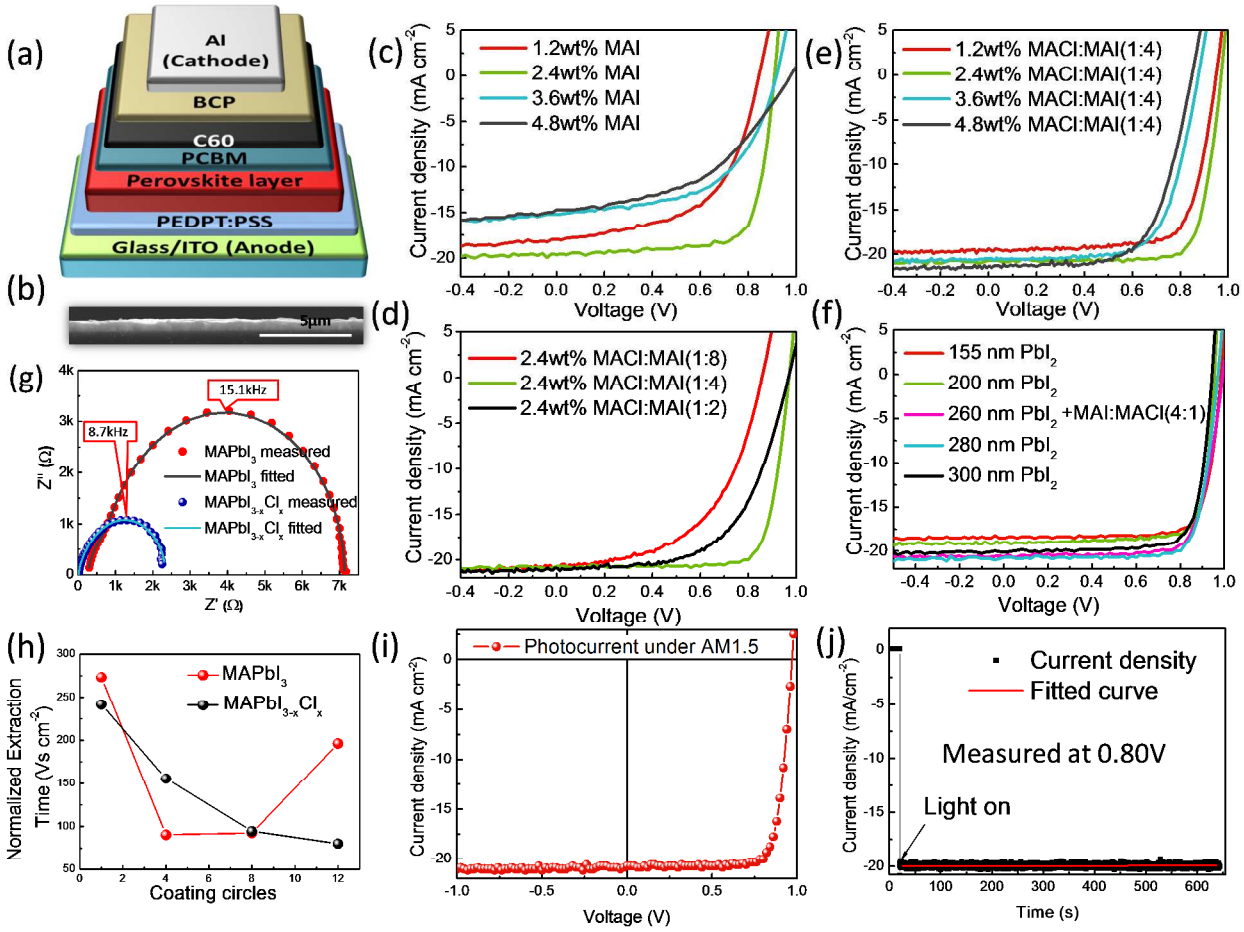

Figure 3. *Q. Dong et al*

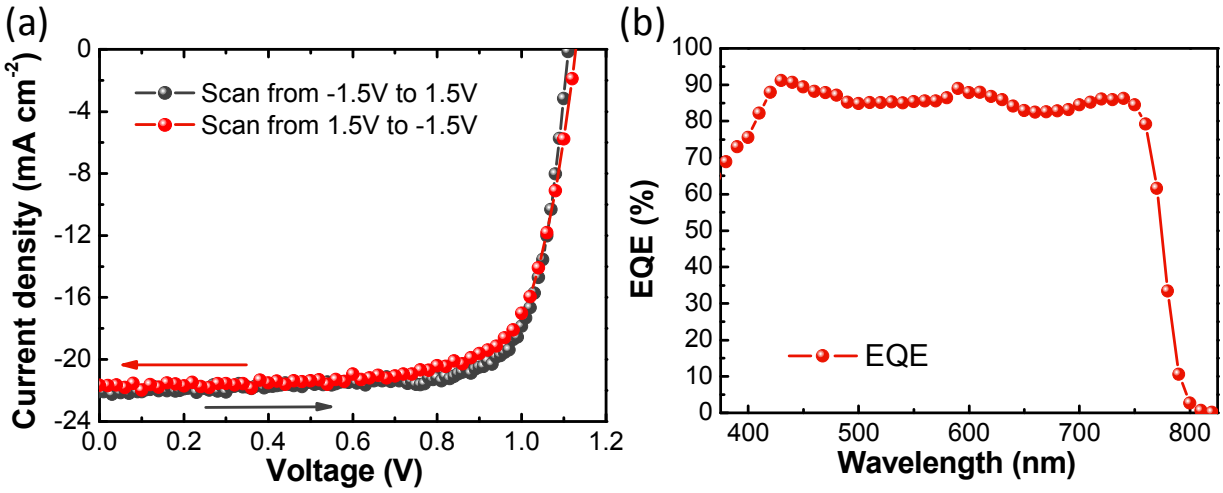

Figure 4. *Q. Dong et al*

Broader context

We report that the incorporation of Cl in precursor in the form of MAI:MACl for mixed halide perovskite formation by a multi-cycle coating interdiffusion method can induce the abnormal grain growth behavior, form large size perovskite grains. The large grain size is found to contribute mainly to a longer carrier recombination lifetime, but without significantly impacting the carrier transport property. High the device power conversion efficiency was increased to 18.9 %, and the devices showed no photocurrent hysteresis. Using the multi-cycle interdiffusion method, a strong correlation was observed between the abnormal grain growth, grain lateral size/thickness ratio enhancement and carrier lifetime/diffusion length increase. The multi-cycle interdiffusion process is a new method to fabricate mixed halide perovskite films different from the single step method reported previously in its different capability in controlling morphology and microstructures. The study presented here pointed out a new direction to produce very large size grains by abnormal grain growth mechanism, which is crucial to achieve high efficiency polycrystalline thin film solar cells because reduced grain boundary area can effectively suppress charge recombination.